PERFORMANCE EVALUATION OF 40 CM ION OPTICS FOR THE NEXT ION ENGINE

George C. Soulas, Thomas W. Haag, and Michael J. Patterson
NASA Glenn Research Center
Cleveland, OH

The results of performance tests with two 40 cm ion optics sets are presented and compared to those of 30 cm ion optics with similar aperture geometries. The 40 cm ion optics utilized both NSTAR and TAG (Thick-Accelerator-Grid) aperture geometries. All 40 cm ion optics tests were conducted on a NEXT (NASA's Evolutionary Xenon Thruster) laboratory model ion engine. Ion optics performance tests were conducted over a beam current range of 1.20-3.52 A and an engine input power range of 1.1-6.9 kW. Measured ion optics' performance parameters included near-field radial beam current density profiles, impingement-limited total voltages, electron backstreaming limits, screen grid ion transparencies, beam divergence angles, and start-up transients. Impingement-limited total voltages for 40 cm ion optics with the NSTAR aperture geometry were 60-90 V lower than those with the TAG aperture geometry. This difference was speculated to be due to an incomplete burn-in of the TAG ion optics. Electron backstreaming limits for the 40 cm ion optics with the TAG aperture geometry were 8-19 V higher than those with the NSTAR aperture geometry due to the thicker accelerator grid of the TAG geometry. Because the NEXT ion engine provided beam flatness parameters that were 40-63% higher than those of the NSTAR ion engine, the 40 cm ion optics outperformed the 30 cm ion optics.

Introduction

The NASA Glenn Research Center (GRC) is developing a next generation ion propulsion system to follow the NSTAR propulsion system. This ion propulsion system, called NASA's Evolutionary Xenon Thruster (or NEXT), includes a 40 cm diameter ion engine. Ion engine performance goals include, in part, a 1–7 kW power-throttling envelope, a specific impulse capability of over 4000 seconds, and a near 70% efficiency for deep-space applications.[1]

The NEXT 40 cm ion engine has twice the beam area as the NSTAR ion thruster, whose beam diameter is approximately 28 cm. The technical approach utilized by the NEXT design is a continuation of the "derating" philosophy used for the NSTAR ion engine. With regards to the ion optics, this approach maintains low beam current densities across the ion optics to extend ion optics' service life. The 40 cm ion optics can further offer increased input power and propellant throughput when other grid technologies are used, such as thick-accelerator-grid (or TAG) ion optics.[2]

A preliminary analysis was conducted in Ref. 3 to determine an appropriate design for and predict the performance of the 40 cm ion optics. NSTAR and TAG aperture geometries and material were selected so that the large performance and service life database already available could be utilized. A preliminary throttle table for the 40 cm ion thruster was developed based, in part, on the predicted performance of the ion optics' aperture geometries. Dome-shaped grids were chosen for the design of the 40 cm ion optics because they are naturally suited for large-area ion optics. A dome height-to-chord radius ratio similar to that of the NSTAR grids was further utilized because it addressed most key issues associated with grid fabrication and thruster operation. A preliminary service life assessment was conducted to determine the lifetime gain by utilizing larger area ion optics. Although a 40 cm ion optics set had been successfully fabricated, all performance test results reported in Ref. 3 were conducted with 50 cm ion optics from a prior program.

This paper reports on the results of performance tests with two 40 cm molybdenum ion optics assemblies and compares them to those of 30 cm molybdenum ion optics with similar aperture geometries.[2,4] One 40 cm ion optics assembly utilized the NSTAR aperture geometry and the other the TAG aperture geometry. All 40 cm ion optics tests were conducted on a NEXT laboratory model ion thruster. Ion optics performance tests were conducted over a beam current range of 1.20-3.52 A and a engine input power range of 1.1-6.9 kW. Measured ion optics' performance parameters included near-field beam current density profiles, impingement-limited total voltages, electron backstreaming limits,

screen grid ion transparencies, beam divergence angles, and start-up transients.

Test Hardware and Operating Procedures

40 cm Ion Optics

NSTAR Aperture Geometry

A photograph of 40 cm grids is shown in Fig. 1, with a 30 cm grid for comparison. The 40 cm ion optics set that utilized the NSTAR aperture geometry had pretest screen and accelerator grid aperture diameter variations within +1%/-8% and +7%/-2%, respectively, of the nominal design throughout the active area (i.e. the perforated area).[5,6] The resulting screen grid open area fraction was estimated to be 8% lower than the nominal design.

These grids were mounted onto a 40 cm engineering model ion optics mounting assembly, as shown in Fig. 2. Pretest grid cold gap variations throughout the active area were measured to be within approximately +4%/-8% of the nominal design. Screen and accelerator grid aperture alignment was checked with microscope and was found to be less than 4% of the nominal cold grid gap.

TAG Aperture Geometry

The TAG aperture geometry is similar to the NSTAR aperture geometry, except that the accelerator grid is 50% thicker to improve ion optics service life.[2] The 40 cm ion optics set that utilized the TAG aperture geometry had pretest screen and accelerator grid aperture diameter variations within ±3% and +4%/-16%, respectively, of the nominal design throughout the active area.[2] The resulting screen grid open area fraction was estimated to be within 1% of the nominal design.

These grids were also mounted onto a 40 cm engineering model ion optics mounting assembly, as shown in Fig. 2. Pretest grid cold gap variations throughout the active area were measured to be within approximately +4%/-0% of the nominal design. Screen and accelerator grid aperture alignment was checked with microscope and was found to be within 4% of the nominal cold grid gap.

Ion Engine

The ion optics sets were mounted onto a NEXT laboratory model (LM) ion engine, which is shown in Fig. 3 and described in detail in Ref. 1. This engine utilized a hollow cathode electron emitter and a ring-cusp magnetic circuit for improved discharge losses at high propellant utilization efficiencies. For the tests reported herein, the NEXT LM ion engine utilized a laboratory model NSTAR neutralizer.

Power Console and Gas Feed System

A power console similar to that described in Ref. 7 powered the thruster. This power console allows for ion engine input powers of over 10 kW with beam power supply voltages of up to 2000 V. A high purity gas feed system was used to provide xenon to the discharge cathode, discharge chamber, and neutralizer through separate mass flow controllers.

Diagnostics

During thruster operation, voltages and currents were measured with digital multimeters and xenon flows with mass flow meters. These measured parameters were used to set engine operating conditions, as well as to determine engine performance.

The engine was connected to an electrically floating power supply circuit used to determine the screen grid transparency to discharge chamber ions. The circuit electrically tied the screen grid to the discharge cathode during normal operation, but biased the grid negative relative to discharge cathode potential to repel electrons and measure the collected ion current.

Beam current density profiles were measured with a probe mounted onto a two-axis probe motion system. The probe was a planar geometry with a 1 cm^2 circular current-collecting area. The probe was biased negative with respect to beam plasma potential to repel electrons and was grounded through a resistor that acted as a shunt to measure collected currents.

The positioning system swept the probe in the radial and axial directions through the vertical center of the engine ion optics. The positioning system had a 1.25 m maximum travel in each axis, which enabled near-field radial beam current density measurements at different axial locations, as measured from the geometric center of the ion optics. The current density measurements were then used to determine radial beam current density profiles, beam divergence half-angles, and thrust correction factors.[8]

Vacuum Facility

Testing was conducted in Vacuum Facility 11 at NASA GRC. This 2.2 m diameter × 7.9 m long facility is evacuated with seven cryogenic pumps and a turbomolecular pump. The total measured facility

pumping speed was greater than 100,000 l/s with xenon. The facility base pressure for these tests was typically about 4×10^{-5} Pa (3×10^{-7} Torr).

Facility background pressures during testing were less than 9.3×10^{-4} Pa (7×10^{-6} Torr), except at the highest beam current. During operation at the highest beam current, the high xenon flow rates and beam power tended to warm-up three of the seven cryogenic pumps. This reduced the facility's effective pumping speed, and resulted in background pressures that increased with operating time up to 1.6×10^{-3} Pa (1.2×10^{-5} Torr).

Operating Procedures

During each ion optics test, the engine was operated at beam currents of 1.20, 2.00, 2.70, and 3.52 A. At each beam current, the beam and accelerator voltages were varied to determine engine and ion optics performance. Ion engine input power, beam voltages, accelerator voltages, total voltages, beam currents, discharge chamber xenon flows, and specific impulses are listed in Table 1. At each operating condition, ion optics performance parameters such as impingement-limited total voltages, electron backstreaming limits, screen grid ion transparencies, as well as other thruster performance parameters, were determined. Beam current densities were only measured with the 40 cm ion optics with the NSTAR aperture geometry. After the performance of the engine and ion optics were characterized, the thermally induced effects of engine startup on the ion optics hot gap were assessed.[8]

A prior studies found that new 30 cm TAG ion optics' performance parameters, which included perveance, electron backstreaming, and screen grid ion transparency, could initially change rapidly with accumulated engine operation until finally achieving steady state values, termed an ion optics burn-in.[2] No attempt was made in this study, however, to operate either 40 cm ion optics set until performance parameters achieved steady state values.

Results and Discussions

The following sections present and discuss ion optics performance test results for 40 cm ion optics with the NSTAR and TAG ion optics aperture geometries. Results are also compared to those with 30 cm ion optics with the same nominal aperture geometries.

Near-field Radial Beam Current Density Profiles

Near-field radial beam current density profiles were used to determine radial current density distributions and peak current densities for data comparisons. Regarding beam current density measurements, no attempt was made to repel charge-exchange ions from the probe or to account for secondary electron emission due to ion bombardment. Integration of the radial beam current density profiles (assuming azimuthal symmetry) yielded beam currents that were higher than the measured beam current by as much as 15%. Possible sources of error are discussed in Refs. 2, 4, and 8.

Sample radial beam current density distributions are shown in Fig. 4 for the 40 cm ion optics with the NSTAR aperture geometry. As the figure demonstrates, the beam current density profiles were similar at all beam currents evaluated. The radial profiles were also non-axisymmetric near the center. This asymmetry is an artifact of the engine discharge chamber plasma and has been noticed with NSTAR ion engines.[2,4,8]

Radial beam current density profiles for 30 and 40 cm ion optics with the NSTAR aperture geometry are compared in Fig. 5. In this figure, top and bottom radial profile pairs correspond to similar average beam current densities. As the figure shows, the NEXT LM ion engine beam current density profiles were far less peaked than those of the NSTAR engine.

NSTAR and NEXT ion engine beam flatness parameters (i.e. the ratio of average-to-peak beam current density) are compared in Table 2 at similar average beam current densities. The NEXT LM ion engine beam flatness parameters were 40-63% higher than those of the NSTAR ion engine in Ref. 4. As will be discussed in the following sections, these higher flatness parameters increased electron backstreaming limits, and are speculated to have contributed to increases in ion optics perveance and screen grid ion transparencies relative to those of the 30 cm ion optics on an NSTAR engine.

The higher beam flatness parameters of the NEXT LM ion engine can also lead to reduced accelerator aperture enlargement near the grid center. This is because charge-exchange production is directly proportional to the number density of beam ions, which has been significantly reduced near the grid center of this engine. Because accelerator grid aperture enlargement is a primary grid failure mechanism, the higher beam flatness parameters of the NEXT LM ion engine should enhance accelerator grid service life.

Impingement-limited Total Voltage

Impingement-limited total voltage is a measure of ion optics' current extraction capability, and, therefore, a measure of ion optics' perveance. Impingement-limited total voltages were determined from plots of accelerator

current as a function of total voltage where the slope was -0.02 mA/V (i.e. the NSTAR criterion). Total voltage is the sum of the absolute values of the beam and accelerator power supply voltages. Uncertainties in impingement-limited total voltage determinations were estimated to be within ±20 V.

Beam current as a function of impingement-limited total voltage is plotted in Fig. 6 for both NSTAR and TAG aperture geometries of the 40 cm ion optics. As the figure shows, the NSTAR aperture geometry had impingement-limited total voltages that were 60-90 V lower than those of the TAG aperture geometry. Although this difference is relatively small, a past study's comparison of these aperture geometries with 30 cm ion optics found them to be similar.[2] However, in that study, it was also shown that the impingement-limited total voltages for the TAG ion optics decreased by about 80 V as a result of an ion optics burn-in. Furthermore, no burn-in was identified for the NSTAR ion optics. It is, therefore, speculated that the difference between the two aperture geometries for the 40 cm ion optics may have been due, in part, to an incomplete burn-in of the TAG ion optics.

To facilitate comparisons of 30 cm and 40 cm ion optics data, the average beamlet current as a function of impingement-limited total voltage is plotted in Fig. 7 for 30 and 40 cm ion optics with NSTAR and TAG aperture geometries. Data for the 30 cm ion optics data were taken from Refs. 2 and 4. The slopes of the accelerator current as a function of total voltage used to define the impingement-limited total voltage for the 30 and 40 cm ion optics data were -0.02 mA/V and -0.04 mA/V, respectively, to ensure a proper comparison between the two grid diameters. This is because the accelerator current is a measure of the total impingement current throughout the accelerator grid area. Because it is assumed here that all apertures contribute equally to the increasing accelerator current for a decreasing total voltage, doubling the number of apertures would double the slope of the accelerator current versus total voltage. Because the 40 cm ion optics have twice the number of apertures as the 30 cm ion optics, the slope was increased to -0.04 mA/V for this comparison.

As Fig. 7 shows, the 40 cm ion optics with the NSTAR aperture geometry had impingement-limited total voltages that were about 120-150 V lower than those of the 30 cm ion optics sets. Furthermore, the 40 cm ion optics with the TAG aperture geometry also had impingement-limited total voltages that were about 50-80 V lower than those of the 30 cm ion optics sets.

This discrepancy in impingement-limited voltages for the two ion optics' diameters is likely due to differences in beam current density distributions, especially in the region of the peak current density. This was demonstrated in Ref. 4, where the impingement-limited total voltage was shown to be a strong function of the peak beam current density (and, therefore, peak beamlet current) due to the similar beam current density distributions. Unfortunately, comparing differing beam current density distributions, such as those of the NEXT and NSTAR ion engines shown in Fig. 5, is difficult. This is because knowledge of the number of beamlets that contribute to the increasing accelerator current as a function of total voltage is presently unknown. As a result, the selection of appropriate impingement-limited voltage criteria (i.e. slopes of the accelerator current as a function of total voltage) for an ion optics comparison is not possible for these different beam current distributions.

It can be concluded, however, that the higher beam flatness parameters of the NEXT LM ion engine allowed the 40 cm ion optics to outperform the 30 cm ion optics with regards to perveance at similar average beam current densities.

Electron Backstreaming Limit

The electron backstreaming limit is the highest accelerator voltage that will prevent beam plasma electrons from backstreaming through the ion optics. The electron backstreaming limit was determined by lowering the magnitude of the accelerator grid voltage until the indicated beam current increased by 0.1 mA due to backstreaming electrons. Uncertainties in electron backstreaming limit measurements were estimated to be within ±2 V.

Figure 8 compares the electron backstreaming limits of the NSTAR and TAG aperture geometries of the 40 cm ion optics as a function of beam power supply voltage at various beam currents. As the figure demonstrates, the electron backstreaming limits of the TAG aperture geometry were 8-19 V higher than those of the NSTAR geometry due to the thicker accelerator grid of the TAG geometry. In general, the magnitude of the disparity increased with increasing beam power supply voltage and peak beam current density. These two geometries were also compared in Ref. 2 with 30 cm ion optics. In that study, the TAG aperture geometry's electron backstreaming limits were 5-9 V higher than those of the NSTAR geometry at a beam power supply voltage of 1100 V. With the 40 cm ion optics, this disparity was 11-14 V for a 1020 V beam power supply voltage. The disparities of the TAG and NSTAR aperture geometries for the two ion optics' diameters are considered small,

and may either be the result of minor differences in the actual aperture geometry or an incomplete ion optics burn-in of the 40 cm ion optics with the TAG aperture geometry.[2]

Figure 9 compares the electron backstreaming limits of the 30 and 40 cm ion optics with the NSTAR aperture geometry as a function of peak beam current density at various beam power supply voltages. As the figure shows, the 40 cm ion optics generally exhibited similar electron backstreaming limits and trends as a function of peak beam current density as the 30 cm ion optics with the NSTAR aperture geometry. For example, the 1100 V beam voltage curve of 30 cm ion optics exhibited electron backstreaming voltages similar to those of the 40 cm ion optics between 1020 and 1180 V. The 1500 V beam voltage curve of 30 cm ion optics also exhibited electron backstreaming voltages similar to those of the 40 cm ion optics at 1570 V at peak beam current densities greater than 4 mA/cm^2, however, the 30 cm ion optics values were lower at lower peak beam current densities. Regardless, these disparities were small and may have been due to minor differences in the hot gaps of the two ion optics' diameters.

Figure 9 also demonstrates that the 40 cm ion optics can operate at higher electron backstreaming limits than the 30 cm ion optics at similar beam voltages and average beam current densities. This is because the NEXT LM ion engine provided significantly higher beam flatness than the NSTAR ion engine.

Screen Grid Ion Transparency

Screen grid ion transparencies are considered here because they directly impact ion engine discharge losses. Screen grid ion transparencies were determined by biasing the screen grid 20 V below discharge cathode potential to repel electrons and measure the collected ion current. The method used to determine screen grid ion transparency from these measurements is discussed in detail in Ref. 8. Uncertainties in screen grid ion transparency measurements were estimated to be within ±0.002.

Figure 10 compares the screen grid ion transparencies of the NSTAR and TAG aperture geometries of the 40 cm ion optics as a function of beam current at various total voltages. The screen grid ion transparencies of the TAG aperture geometry were 0.7-2.6% greater than those of the NSTAR aperture geometry. The discrepancies generally increased with decreasing total voltage and increasing beam current. The lower transparencies of the NSTAR aperture geometry is likely due to its smaller screen grid open area fraction, which was estimated to be about 8% lower than the nominal design.

Figure 11 compares the screen grid ion transparencies of the 30 and 40 cm ion optics with the NSTAR aperture geometry function of the average beam current density at various total voltages. Plotting the transparency as a function of the average beam current density allowed for comparisons between ion optics with different diameters. As the figure shows, the screen grid ion transparencies of the 30 cm ion optics were within about 3% lower than those of the 40 cm ion optics.

This discrepancy, though small, was not the result of differing screen grid open area fractions because the open area fraction of the 30 cm ion optics was about 5% greater than that of the 40 cm ion optics. Furthermore, the cold grid gaps of the two ion optics' diameters were similar. The discrepancy may have been due to the higher beam flatness parameters of the NEXT LM ion engine. In Fig. 11, the 30 and 40 cm ion optics data at high average beam current densities indicate that screen grid ion transparency decreases with increasing average beam current density. Because the 30 cm ion optics operated with a lower beam flatness (i.e. higher peak beam current densities) than that of the 40 cm ion optics, the resulting screen grid ion transparencies of the 30 cm ion optics were lower.

Regardless, the 40 cm ion optics on the NEXT LM ion engine outperformed the 30 cm ion optics on an NSTAR engine with regards to the screen grid ion transparency.

Beam Divergence and Thrust Losses

Radial beam current density profiles were further taken at 45 axial locations to determine beam divergence half-angles and thrust losses due to beam divergence for the 40 cm ion optics with the NSTAR aperture geometry. The methods used to determine divergence half-angles and thrust losses are discussed in detail in Ref. 8. Uncertainties in the beam divergence half-angles and thrust losses due to beam divergence cannot presently be assessed due to the unknown sources of error in the beam current density measurements.

Table 3 lists the beam divergence half-angles and beam divergence thrust correction factors for the 40 cm ion optics with the NSTAR aperture geometry at a beam power supply voltage of 1570 V. Also listed in Table 3 are 30 cm ion optics results at a beam power supply voltage of 1500 V and at similar average beam current densities. The 30 and 40 cm ion optics were also operated at similar beam-to-total voltage ratios. As the

table shows, 40 cm ion optics' beam divergence half-angles were no more than 3° higher than those of the 30 cm optics. The resulting beam divergence thrust correction factors were within 1% for both ion optics diameters. This similarity was not surprising because the 40 cm ion optics were designed with the same maximum beamlet deflection angle due to the grid dome shape as that of the 30 cm ion optics.[3]

Thermally-Induced Effects During Thruster Startup

The aforementioned test results were obtained with the ion optics thermally at steady state. As a result, the hot gap between the screen and accelerator grids was stable. During thruster startup, however, thermal transients and uneven heating of the screen and accelerator grids cause the grid gap to significantly decrease, then increase to a stable value.[9] As a final test for each 40 cm ion optics set, the ion engine was started from room temperature and operated with beam extraction within 1 minute of discharge ignition. Each 40 cm ion optics set was operated at a 3.52 A beam current and 1180 V beam power supply voltage. The objective was to use temporal electron backstreaming limit changes to gain insight into the hot grid gap changes, as was done in Ref. 10.

The results of these tests are shown in Fig. 12, along with data with 30 cm ion optics for comparison. The 30 cm ion optics were operated on an NSTAR ion engine at a 1.76 A beam current (i.e. the same average beam current density as the 40 cm ion optics) and 1100 V beam power supply voltage. The figure shows that electron backstreaming limits for both 40 cm ion optics geometries were within 2 V of their steady state values 40-50 minutes after ignition. Electron backstreaming limits for the 30 cm ion optics set were within 2 V of the steady state value about 35-40 minutes after ignition. These results indicate that the hot grid gap likely stabilizes within about 40-50 minutes from discharge ignition for the 40 cm ion engine and 35-40 minutes for the 30 cm ion optics. No anomalies were detected during these tests.

It is interesting to note that while the electron backstreaming limits of the 30 cm ion optics monotonically increased until the steady state value was reached, the measured backstreaming limits of both 40 cm ion optics initially operated at near constant values, then increased to final steady state values. The cause for this behavior is presently unknown.

Post-test Ion Optics Inspection

Following these performance tests, both 40 cm ion optics sets were removed and re-inspected. Measured post-test dimensions included aperture diameters and the cold grid gap.

Post-test screen and accelerator aperture diameters for both 40 cm ion optics aperture geometries showed no measurable change as a result of performance testing. This was not surprising given the short duration of these tests. The cold grid gap of the 40 cm ion optics with the NSTAR aperture geometry also showed no measurable change. The cold grid gap of the 40 cm ion optics with the TAG aperture geometry, however, decreased about 8% throughout the entire active area. This change was also noted with the 30 cm ion optics at the active area center in Ref. 2. The cause of this change, while small, is not yet understood.

Conclusions

The results of performance tests with two 40 cm ion optics sets were presented. The 40 cm ion optics utilized both NSTAR and TAG geometries. All 40 cm ion optics tests were conducted on a NEXT laboratory model ion engine.

Performance results with the two 40 cm ion optics' aperture geometries were compared to each other. Impingement-limited total voltages for 40 cm ion optics with the NSTAR aperture geometry were 60-90 V lower than those with the TAG aperture geometry. This difference, though small, was speculated to be due to an incomplete burn-in of the TAG ion optics. Electron backstreaming limits for the 40 cm ion optics with the TAG aperture geometry were 8-19 V higher than those with the NSTAR aperture geometry due to the thicker accelerator grid of the TAG geometry. Screen grid ion transparencies of the 40 cm ion optics with the TAG aperture geometry were 0.7-2.6% greater than those of the NSTAR aperture geometry due to the 8% smaller open area fraction of the NSTAR aperture geometry's screen grid.

Performance results with the 40 cm ion optics were compared to those of 30 cm ion optics with similar aperture geometries. The NEXT LM ion engine provided beam flatness parameters that were 40-63% lower than those of the NSTAR ion engine. As a result, the 40 cm ion optics could be operated with higher electron backstreaming limits and screen grid ion transparencies, and lower impingement-limited total voltages than the 30 cm ion optics.

The 40 cm ion optics' beam divergence half-angles were no more than 3° higher than those of the 30 cm optics. The resulting beam divergence thrust correction factors were within 1% for both ion optics diameters. This similarity was expected because the 40 cm ion

optics were designed with the same maximum beamlet deflection angle due to the grid dome shape as that of the 30 cm ion optics.

Temporal changes in the electron backstreaming limit during thruster startup from room temperature were measured to gain insight into the hot grid gap changes. Results indicate that the hot grid gap stabilized within about 40-50 minutes from discharge ignition, as opposed to 35-40 minutes for the 30 cm ion optics. No anomalies were detected during these tests.

References

[1] Patterson, M.J., et al., "NEXT: NASA's Evolutionary Xenon Thruster," AIAA Paper 2002-3832, July 2002.

[2] Soulas, G.C., "Improving the Total Impulse Capability of the NSTAR Ion Thruster with Thick-Accelerator-Grid Ion Optics," IEPC Paper 01-081, October 2001.

[3] Soulas, G.C., "Design and Performance of 40 cm Ion Optics," IEPC Paper 01-090, October 2001.

[4] Soulas, G.C., "Performance Evaluation of Titanium Ion Optics for the NASA 30 cm Ion Thruster," IEPC Paper 01-092, October 2001.

[5] Christensen, J.A., et al., "Design and Fabrication of a Flight Model 2.3 kW Ion Thruster for the Deep Space 1 Mission," AIAA Paper 98-3327, July 1998.

[6] Sovey, J.S., et al., "Development of an Ion Thruster and Power Processor for New Millenium's Deep Space 1 Mission," AIAA Paper 97-2778, December 1997.

[7] Pinero, L.R., Patterson, M.J., and Satterwhite, V.E., "Power Console Development for NASA's Electric Propulsion Outreach Program," IEPC Paper 93-250, September 1993.

[8] Soulas, G.C., "Performance of Titanium Optics on a NASA 30 cm Ion Thruster," AIAA Paper 2000-3814, July 2000.

[9] MacRae, G.S., Zavesky, R.J., and Gooder, S.T., "Structural and Thermal Response of 30 cm Diameter Ion Thruster optics," AIAA Paper 89-2719, July 1989.

[10] Soulas, G.C., Haag, T.W., Patterson, M.J., and Rawlin, V.K., "Titanium Optics for Ion Thrusters," IEPC Paper 99-149, October 1999.

Table 1. Nominal ion engine operating parameters.

Input Power,[a] kW	Beam Current, A	Beam Voltage,[b] V	Accelerator Voltage, V	Total Voltage, V	Discharge Chamber Flow, sccm	Specific Impulse, sec
6.9	3.52	1800[c]	-298	2100	54.5	4060
6.1	3.52	1570	-257	1820	54.5	3750
5.5	3.52	1400	-243	1640	54.5	3570
4.7	3.52	1180	-227	1410	54.5	3250
5.3	2.70	1800[c]	-298	2100	41.8	3950
4.7	2.70	1570	-257	1820	41.8	3690
4.2	2.70	1400	-243	1640	41.8	3480
3.6	2.70	1180	-227	1410	41.8	3200
3.2	2.70	1020	-216	1240	41.8	2970
4.0	2.00	1800[c]	-298	2100	31.0	3970
3.5	2.00	1570	-257	1820	31.0	3700
3.2	2.00	1400	-243	1640	31.0	3490
2.7	2.00	1180	-227	1410	31.0	3200
2.4	2.00	1020	-216	1240	31.0	2980
2.4	1.20	1800[c]	-298	2100	19.2	3770
2.2	1.20	1570	-257	1820	19.2	3510
1.9	1.20	1400	-243	1640	19.2	3310
1.7	1.20	1180	-227	1410	19.2	3040
1.5	1.20	1020	-216	1240	19.2	2830
1.1	1.20	680	-197	880	19.2	2300

[a]Nominal values.
[b]Power supply voltage.
[c]Only the 40 cm ion optics with the NSTAR aperture geometry were operated at this beam power supply voltage.

Table 2. Beam flatness parameters of the NEXT and NSTAR ion engines at similar average beam current densities. Beam flatness parameters were defined as the average beam current density at the ion optics divided by the peak beam current density measured 45-48 mm downstream of the ion optics center. NSTAR ion engine data are from Ref. 4 with molybdenum ion optics.

Beam Current, A		Beam Flatness Parameter	
NEXT Engine	NSTAR Engine	NEXT Engine	NSTAR Engine
3.52	1.76	0.66	0.47
2.70	1.30	0.63	0.42
2.00	1.10	0.60	0.40
1.20	0.71	0.57	0.35

Table 3. Divergence half-angles at 95% of total beam current and beam divergence thrust correction factors for 40 cm ion optics with the NSTAR aperture geometry. The 40 cm ion optics data were collected at a 1570 V beam power supply voltage. The 30 cm ion optics data were from Ref. 4 with similar average beam current densities for a 1500 V beam power supply voltage.

40 cm Beam Current, A	Average Beam Current Density, mA/cm^2	Divergence Half-Angle at 95% of Beam Current, degrees		Thrust Correction Factor for Beam Divergence	
		40 cm Ion Optics	30 cm Ion Optics	40 cm Ion Optics	30 cm Ion Optics
3.52	2.8	30	29	0.97	0.97
2.70	2.1	32	29	0.96	0.97
2.00	1.6	32	29	0.96	0.97
1.20	1.0	31	29	0.96	0.96

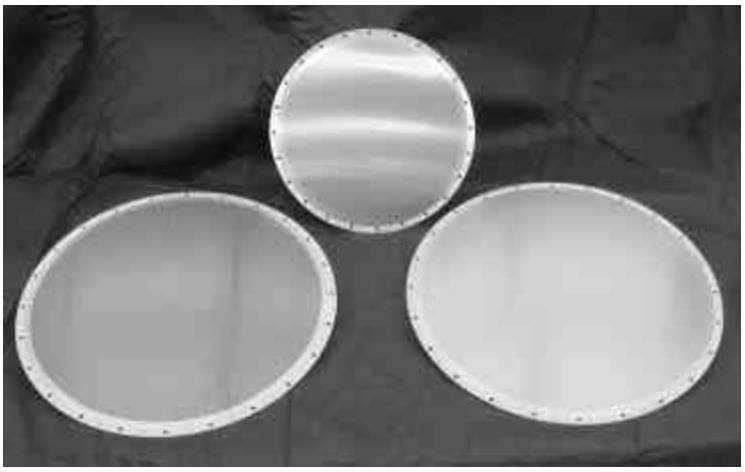

Fig. 1. Photograph of 40 cm screen grid (left foreground) and 40 cm accelerator grid (right foreground) with a 30 cm accelerator grid (center background) for comparison.

Fig. 2. Photograph of 40 cm ion optics installed onto a 40 cm engineering model mounting assembly.

Fig. 3. Photograph of the 40 cm NEXT laboratory model ion engine with ion optics installed.

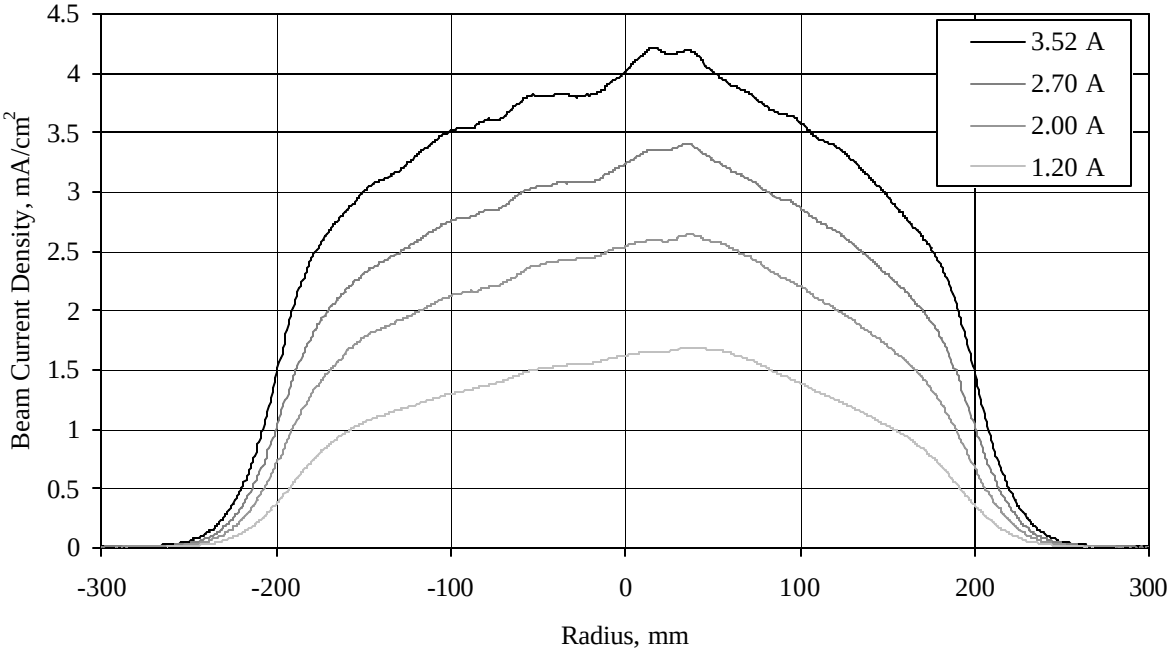

Fig. 4. Radial beam current density profiles for the 40 cm ion optics with the NSTAR aperture geometry at a beam power supply voltage of 1570 V and various beam currents. Profiles were measured 45 mm downstream of the accelerator grid center.

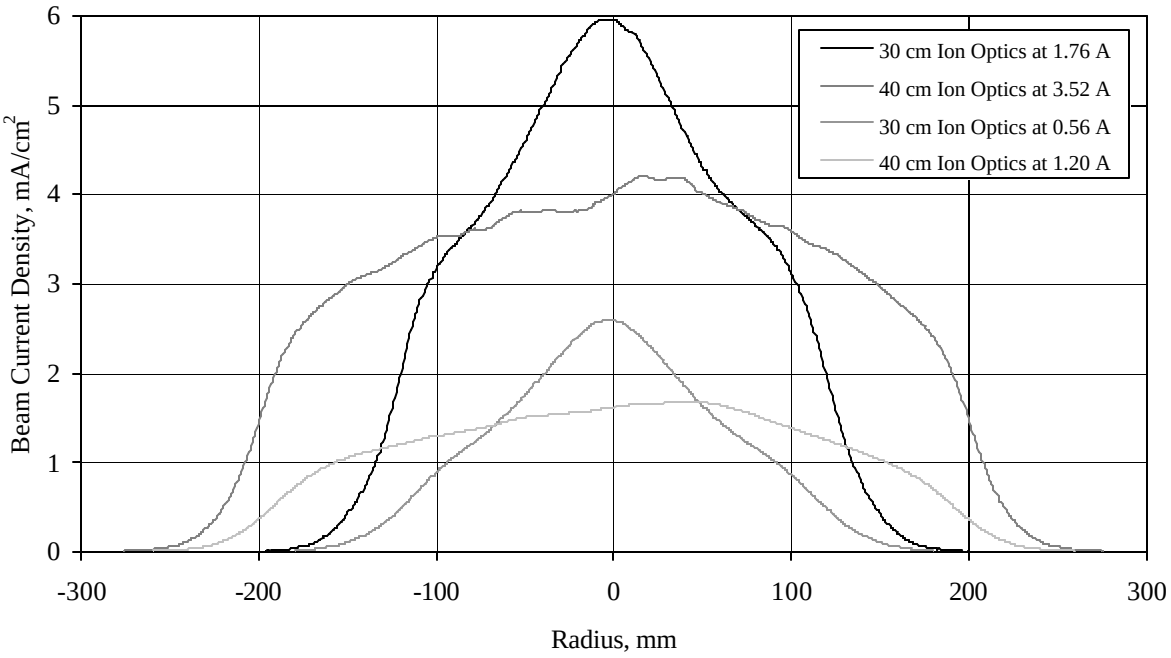

Fig. 5. Radial beam current density profiles for 30 and 40 cm ion optics with the NSTAR aperture geometry at various beam currents. Profiles for the 30 and 40 cm ion optics were measured 48 and 45 mm, respectively, downstream of the accelerator grid center. The top and bottom pairs of radial profiles correspond to average beam current densities of about 2.8 and 1.0 mA/cm^2, respectively. The 30 cm ion optics data are the molybdenum ion optics results from Ref. 4.

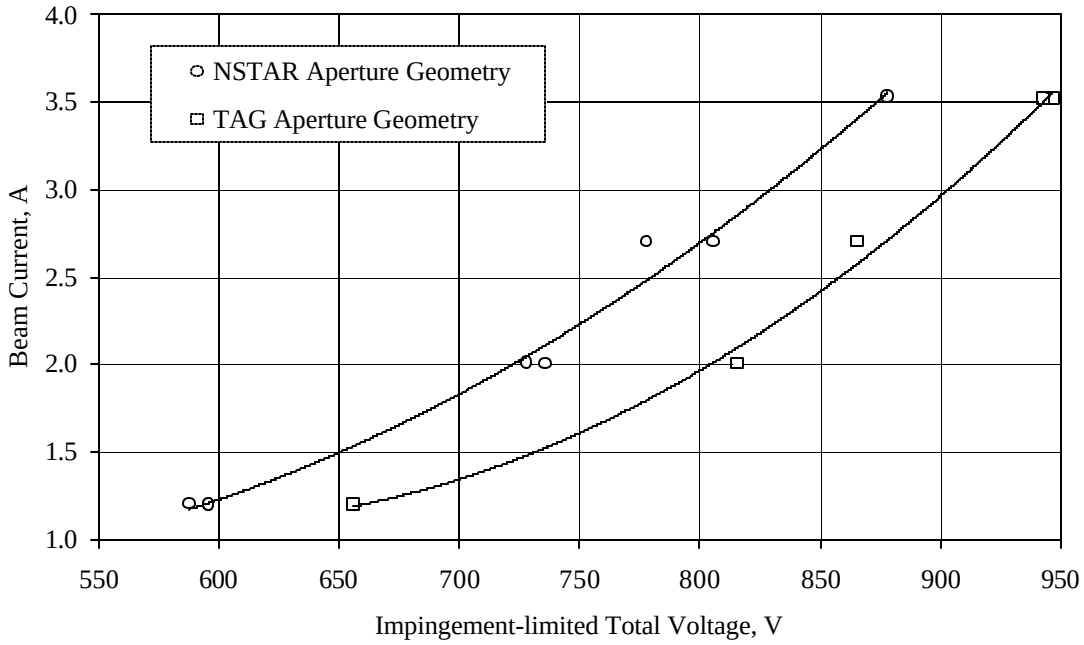

Fig. 6. Beam current as a function of impingement-limited total voltage for 40 cm ion optics with NSTAR and TAG aperture geometries.

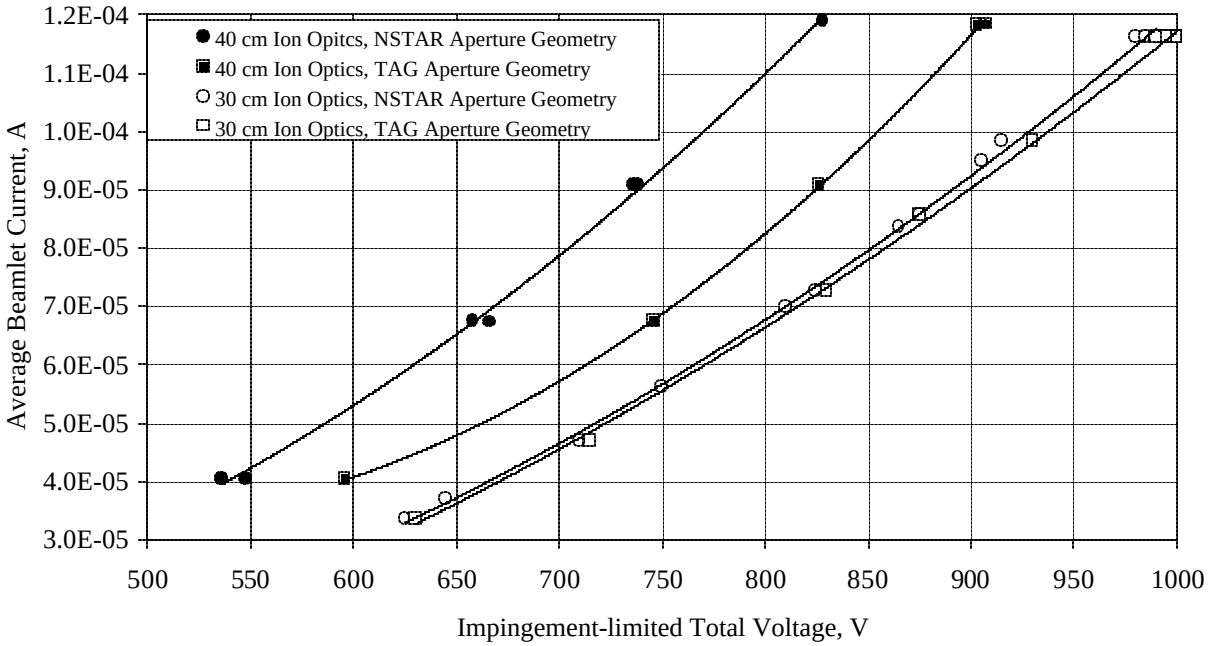

Fig. 7. Average beamlet current as a function of impingement-limited total voltage for 30 and 40 cm ion optics with NSTAR and TAG aperture geometries. The 30 cm ion optics data are the molybdenum ion optics results from Refs. 2 and 4.

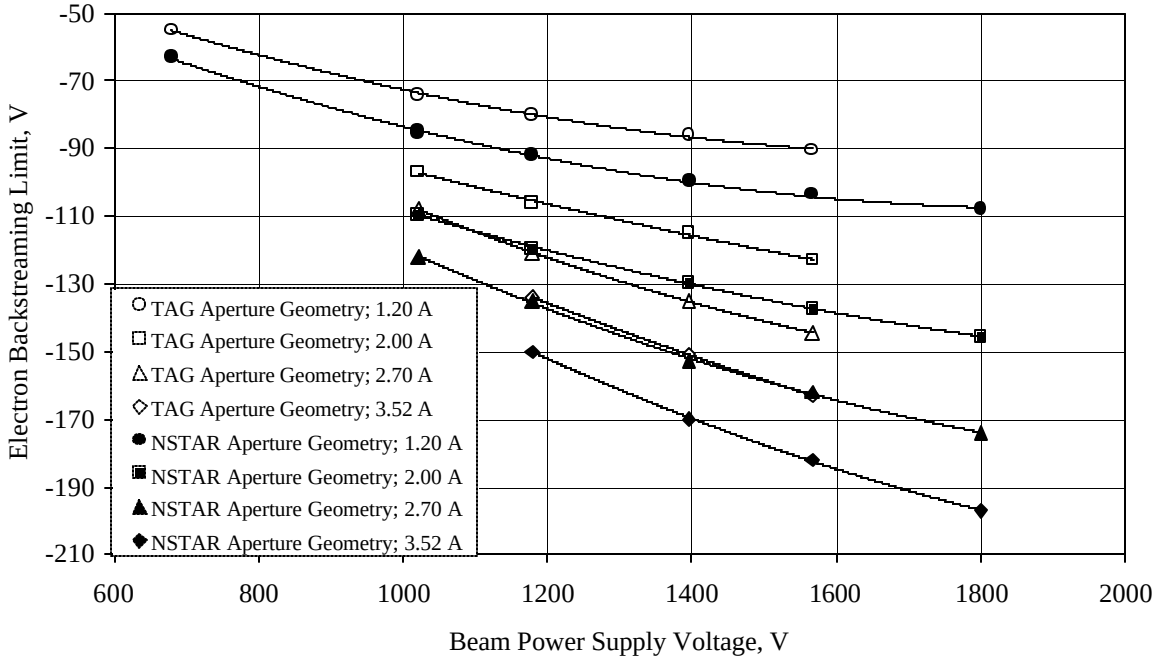

Fig. 8. Electron backstreaming limit as a function of beam power supply voltage at various beam currents for 40 cm ion optics with NSTAR and TAG aperture geometries.

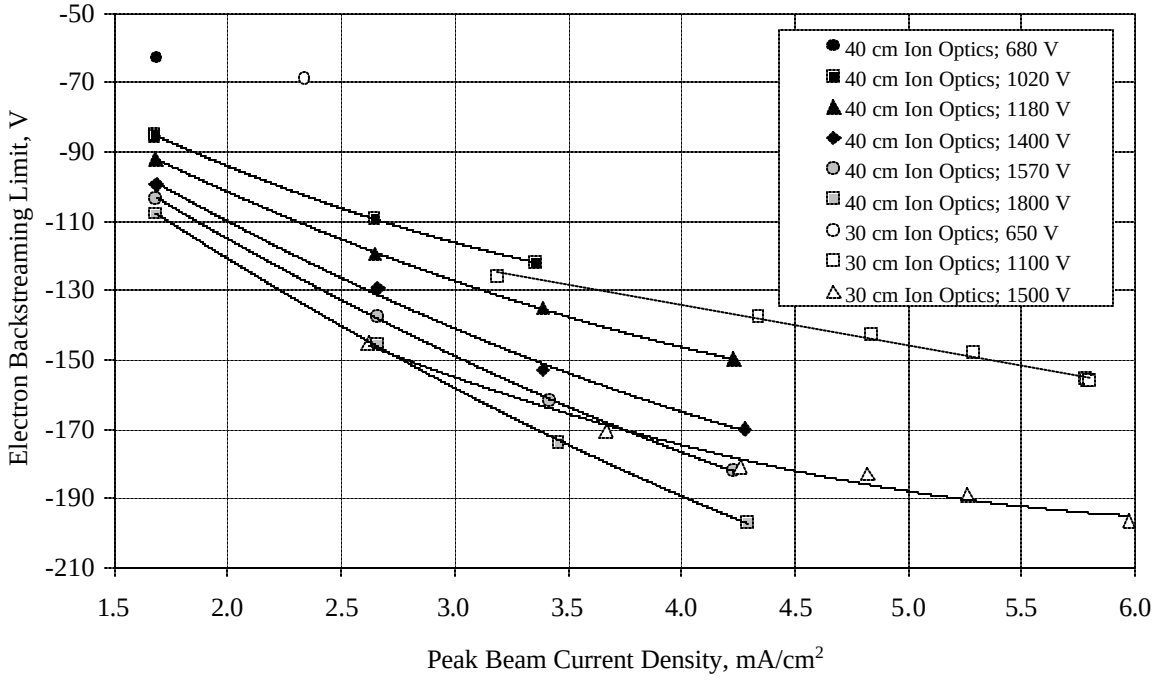

Fig. 9. Electron backstreaming limit as a function of peak beam current density at various beam power supply voltages for 30 and 40 cm ion optics with NSTAR aperture geometry. The 30 cm ion optics data are the molybdenum ion optics results from Ref. 4.

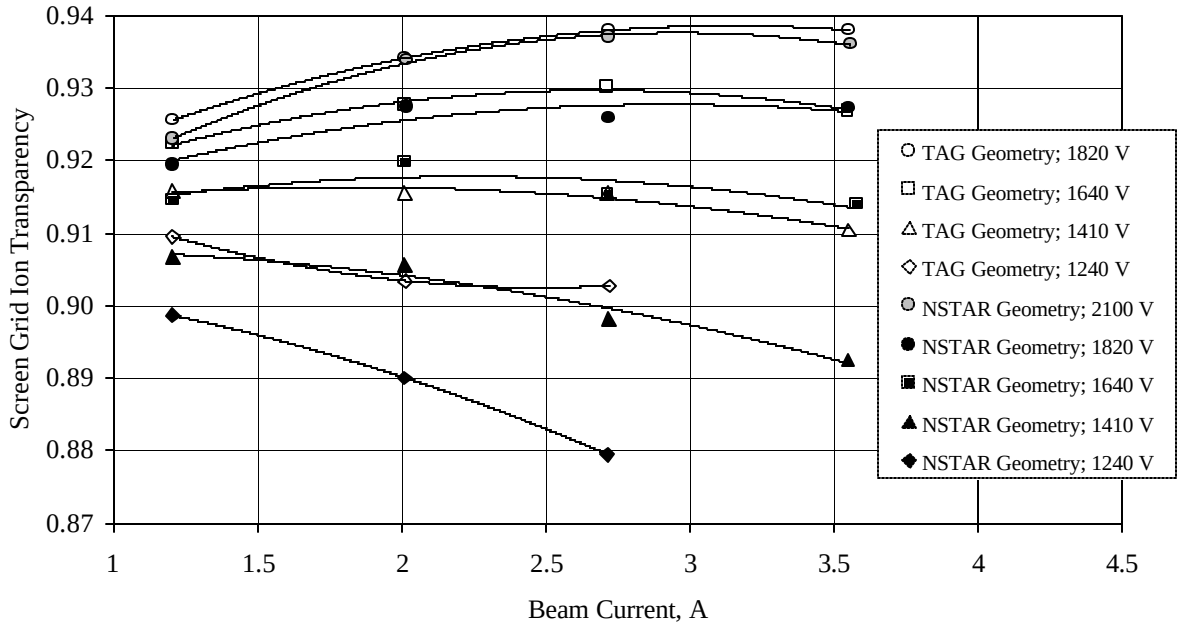

Fig. 10. Screen grid ion transparencies as a function of beam current at various total voltages for 40 cm ion optics with NSTAR and TAG aperture geometries.

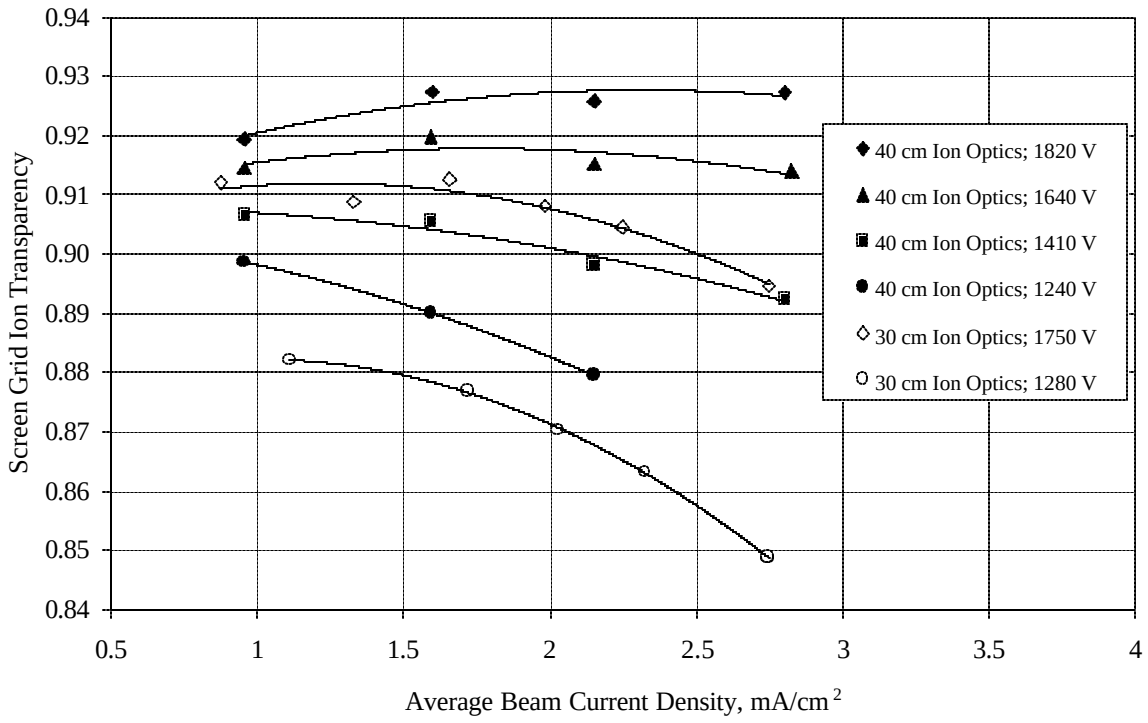

Fig. 11. Screen grid ion transparencies as a function of the average beam current density at various total voltages for 30 and 40 cm ion optics with the NSTAR aperture geometry. The 30 cm ion optics data are the molybdenum ion optics results from Ref. 4.

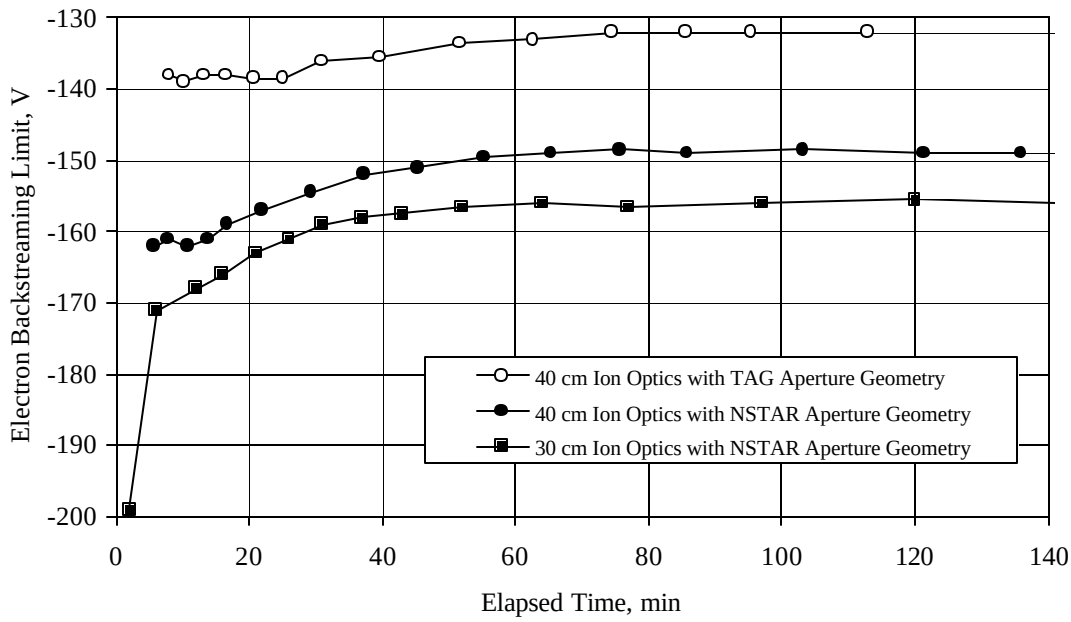

Fig. 12. Electron backstreaming limit as a function of elapsed time for 30 and 40 cm ion optics at 1.76 and 3.52 A beam currents, respectively, and 1100 and 1180 V beam power supply voltages, respectively.